LETTERS

nature cell biology

Arp2/3 ATP hydrolysis-catalysed branch dissociation is critical for endocytic force generation

Adam C. Martin[1], Matthew D. Welch[1] and David G. Drubin[1,2]

The Arp2/3 complex, which is crucial for actin-based motility, nucleates actin filaments and organizes them into y-branched networks. The Arp2 subunit has been shown to hydrolyse ATP, but the functional importance of Arp2/3 ATP hydrolysis is not known. Here, we analysed an Arp2 mutant in *Saccharomyces cerevisiae* that is defective in ATP hydrolysis. Arp2 ATP hydrolysis and Arp2/3-dependent actin nucleation occur almost simultaneously. However, ATP hydrolysis is not required for nucleation. In addition, Arp2 ATP hydrolysis is not required for the release of a WASP-like activator from y-branches. ATP hydrolysis by Arp2, and possibly Arp3, is essential for efficient y-branch dissociation *in vitro*. In living cells, both Arp2 and Arp3 ATP-hydrolysis mutants exhibit defects in endocytic internalization and actin-network disassembly. Our results suggest a critical feature of dendritic nucleation in which debranching and subsequent actin-filament remodelling and/or depolymerization are important for endocytic vesicle morphogenesis.

Actin-filament assembly generates forces that support processes such as cell motility and endocytosis[1,2]. Cycles of actin assembly and disassembly are driven, in part, by the free energy derived from actin ATP hydrolysis. ATP-bound actin polymerizes into filaments and subsequent ATP hydrolysis and release of inorganic phosphate (P_i) destabilizes the filament, promoting depolymerization and recycling of actin subunits. As with actin, ATP binding by the Arp2 and Arp3 subunits of the Arp2/3 complex is critical for the function of this complex[3–6]. However, the function of ATP hydrolysis by the Arp2/3 complex is not clear. Arp2 hydrolyses ATP when a Wiscott-Aldrich syndrome protein (WASP)-family nucleation promoting factor (NPF) activates the Arp2/3 complex and promotes its association with the first actin monomer of the daughter filament[7]. However, depending on the experimental conditions, Arp2 ATP hydrolysis has been observed with half-lives ranging from 20 s (similar to the rate of nucleation)[7] to 800 s (similar to the rate of y-branch dissociation)[8]. Furthermore, studies using non-hydrolysable ATP analogues suggested that Arp2/3 ATP hydrolysis was essential for nucleation[3,4], whereas studies using the ion Cr(III), which is thought to delay Arp2 P_i release following hydrolysis, suggested a role for Arp2 P_i release during y-branch dissociation or debranching[8]. Although Arp3 has not been observed to hydrolyse ATP, residues predicted to catalyse ATP hydrolysis are conserved in Arp3. Importantly, studies using non-hydrolysable ATP analogues and Cr(III) were unable to distinguish whether these molecules affect Arp2, Arp3 or both. In addition, the relevance of Arp2/3 ATP hydrolysis to actin-based force generation in a biological context has not yet been determined. Ideally, Arp2/3 ATP hydrolysis mutants would be used to dissect the *in vitro* mechanism and *in vivo* function of Arp2/3 ATP hydrolysis.

We previously generated 26 mutants that altered conserved residues in the nucleotide-binding pockets of *S. cerevisiae* Arp2 and Arp3 (ref. 6). Two Arp2 mutants were hypothesized to decrease ATP hydrolysis. Here, we focus on $arp2^{H161A}$ as this mutant resulted in a growth defect (see Supplementary Information, Fig. S1a), suggesting impaired Arp2/3 function. The homologous yeast actin histidine (H161) is predicted to activate a water molecule for direct nucleophilic attack on the ATP γ-phosphate[9]. Growth of the corresponding Arp3 mutant, $arp3^{H161A}$, was indistinguishable from wild type. However, $arp3^{H161A}$ was synthetic lethal with $arp2^{H161A}$ (data not shown), demonstrating that $arp3^{H161A}$ also affects Arp2/3 complex function. The H161A mutant phenotypes were not due to reduced protein levels (data not shown), altered Arp2/3 complex subunit composition (see Supplementary Information, Fig. S1b) or a defect in ATP binding (see Supplementary Information, Fig. S1c).

Analysis of Arp2/3 ATP hydrolysis during nucleation is complicated by the fact that actin, which is typically present at a 100-fold molar excess relative to the Arp2/3 complex, hydrolyses ATP soon after polymerization[1,2]. Therefore, an experimental strategy must be used to distinguish between actin, Arp2 and Arp3 ATP hydrolysis. We used an approach in which purified Arp2/3 complex containing Arp2 and Arp3 covalently bound to γ-^{32}P-ATP was used to individually monitor Arp2 and Arp3 γ-phosphate cleavage[7,8]. Yeast Arp2 and Arp3 failed to hydrolyse ATP in the absence of either actin or a WASP-like NPF, Las17p (see Supplementary Information, Fig. S1d). However, the addition of actin and Las17p together resulted in an approximately 50% decrease in the Arp2 ^{32}P-signal over 2 min (Fig. 1a, c). Although a decrease in the Arp3 ^{32}P-signal was not observed, the possibility that crosslinking inactivates

[1]16 Barker Hall, Dept. of Molecular and Cell Biology, University of California Berkeley, CA 94720-3202, USA.
[2]Correspondence should be addressed to D.G.D. (e-mail: drubin@socrates.berkeley.edu)

Received 28 April 2006; accepted 14 June 2006; published online 23 July 2006; DOI: 10.1038/ncb1443

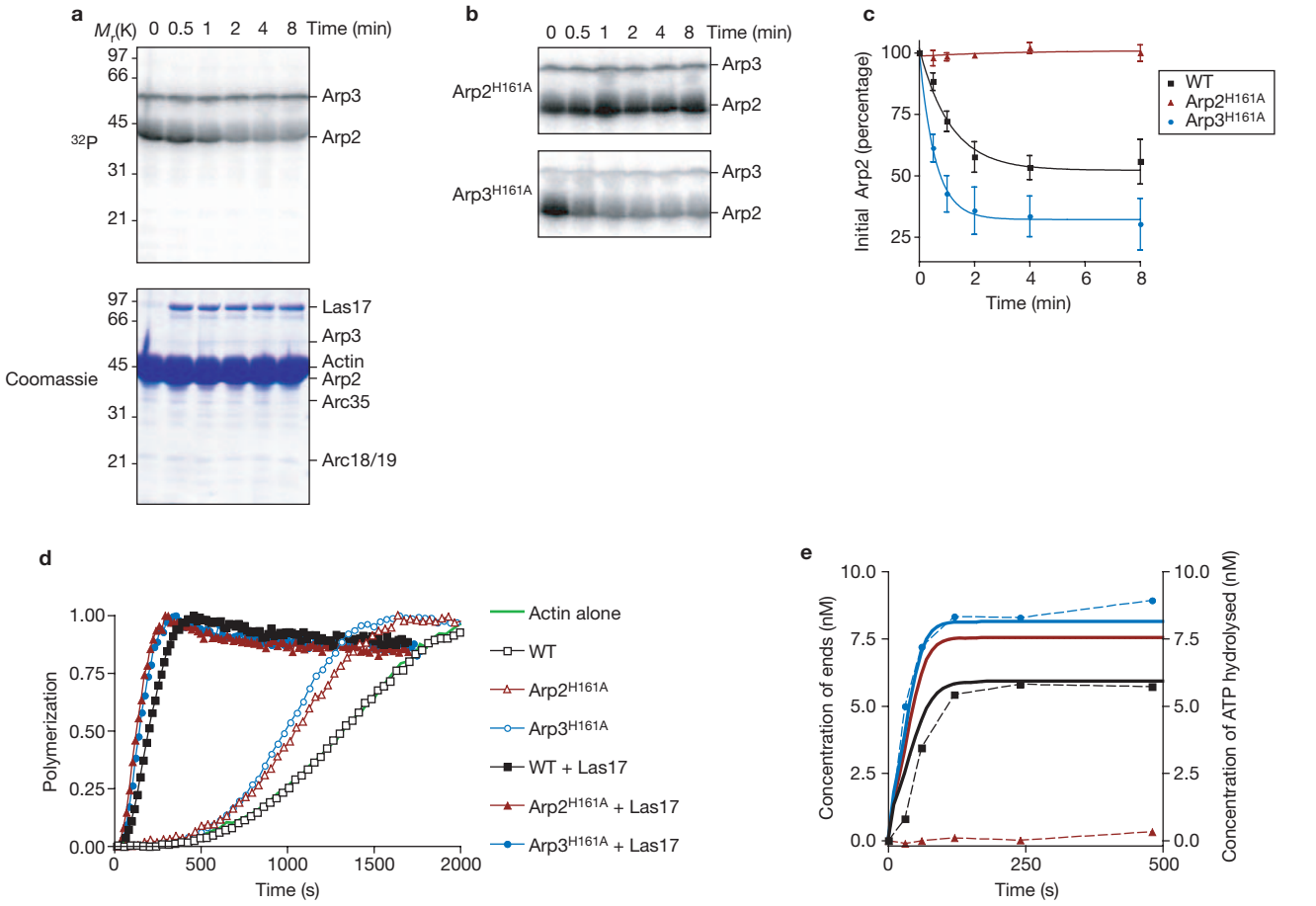

Figure 1 Arp2 ATP hydrolysis is not required for actin filament nucleation. (**a**) Arp2 rapidly hydrolyses ATP on filament nucleation. Yeast Arp2/3 complex was photo-crosslinked to 8-azido-γ-^{32}P-ATP. The γ-^{32}P-ATP-labelled Arp2/3 complex was then used in a nucleation reaction as described in the Methods. Arp2/3 complex subunits were separated by SDS–PAGE and visualized by autoradiography and Coomassie blue stain. (**b**) Arp2 ATP hydrolysis by the H161A mutants. The ATP hydrolysis assay was performed as in **a**, and Arp2 and Arp3 were visualized by autoradiography. The increase in Arp2 ATP hydrolysis by Arp3^{H161A} is due to increased nucleation activity as shown in **d** and **e**. (**c**) Quantification of the decrease in Arp2 ^{32}P signal in different mutants. Data points represent mean ± s.e.m. ($n = 4$ for WT, $n = 3$ for Arp3^{H161A} and $n = 2$ for Arp2^{H161A}). (**d**) Arp2/3 complex containing Arp2^{H161A} efficiently nucleates actin-filament assembly. Actin (2 μM, 10% pyrene-labelled) was polymerized with Arp2/3 complex (40 nM) or Arp2/3 complex (10 nM) and Las17 (10 nM). (**e**) The Arp2^{H161A} mutant uncouples ATP hydrolysis from nucleation. Free barbed-end concentrations for filaments nucleated by Arp2/3 complex (solid lines) were compared with the amount of ATP hydrolysed by Arp2 (symbols and dotted lines). Data for wild type (WT, black), Arp2^{H161A} (red) and Arp3^{H161A} (blue) Arp2/3 complexes are shown.

the ATP hydrolysis activity of Arp3 cannot be excluded. In contrast with wild-type Arp2, Arp2^{H161A} significantly impaired ATP hydrolysis, as indicated by the absence of Arp2^{H161A} γ-phosphate cleavage over 8 min (Fig. 1b, c). Interestingly, Arp2 from the Arp3^{H161A}-mutant complex hydrolysed higher levels of ATP (Fig. 1b, c).

These data suggested that Arp2^{H161A} blocks Arp2 ATP hydrolysis activity. Alternatively, Arp2^{H161A} could impair Arp2/3-mediated nucleation, preventing stimulation of Arp2 ATP hydrolysis. To distinguish between these possibilities, the nucleation activities of Arp2/3 complexes containing either Arp2^{H161A} or Arp3^{H161A} were examined by monitoring pyrene–actin assembly. Arp2^{H161A} and Arp3^{H161A} increased Arp2/3 complex nucleation activity compared with wild type, in both the presence and absence of Las17p (Fig. 1d and see Supplementary Information, Fig. S2a). Furthermore, wild-type and H161A mutant complexes bound to the Arp2/3-binding WCA (WASP homology 2, connector or central, acidic) domain of Las17p with indistinguishable affinity (see Supplementary Information, Fig. S2b). Therefore, the enhanced nucleation activity of these complexes possibly reflects conformational changes that mimic activation, similar to Arp2^{Y306A} (ref. 6). To relate ATP hydrolysis to nucleation activity, free barbed-end concentrations nucleated by the Arp2/3 complex were compared with the amount of Arp2 ATP hydrolysis at different times. Arp2 ATP hydrolysis exhibited a 1:1 correlation with the number of nucleation events for both wild-type and Arp3^{H161A} complexes (Fig. 1e). Thus, the increase in Arp2 ATP hydrolysis observed for Arp3^{H161A} resulted from its higher nucleation activity. Arp2 ATP hydrolysis occurred within 20 s of nucleation for both wild-type and Arp3^{H161A} Arp2/3 complexes. In contrast, Arp2^{H161A} did not hydrolyse ATP, despite efficient nucleation by this Arp2/3 mutant (Fig. 1e). Therefore, Arp2^{H161A} impairs ATP hydrolysis, uncoupling this activity from nucleation. This finding demonstrates that Arp2 ATP hydrolysis is not required for Arp2/3-complex nucleation activity.

In budding yeast, the Arp2/3 complex is required for endocytic internalization[6,10]. Therefore, to determine whether ATP hydrolysis is required for Arp2/3 function *in vivo*, endocytosis of the fluid-phase dye, Lucifer yellow, was examined by fluorescence microscopy. Whereas wild-type cells exhibited intense vacuolar Lucifer yellow staining after

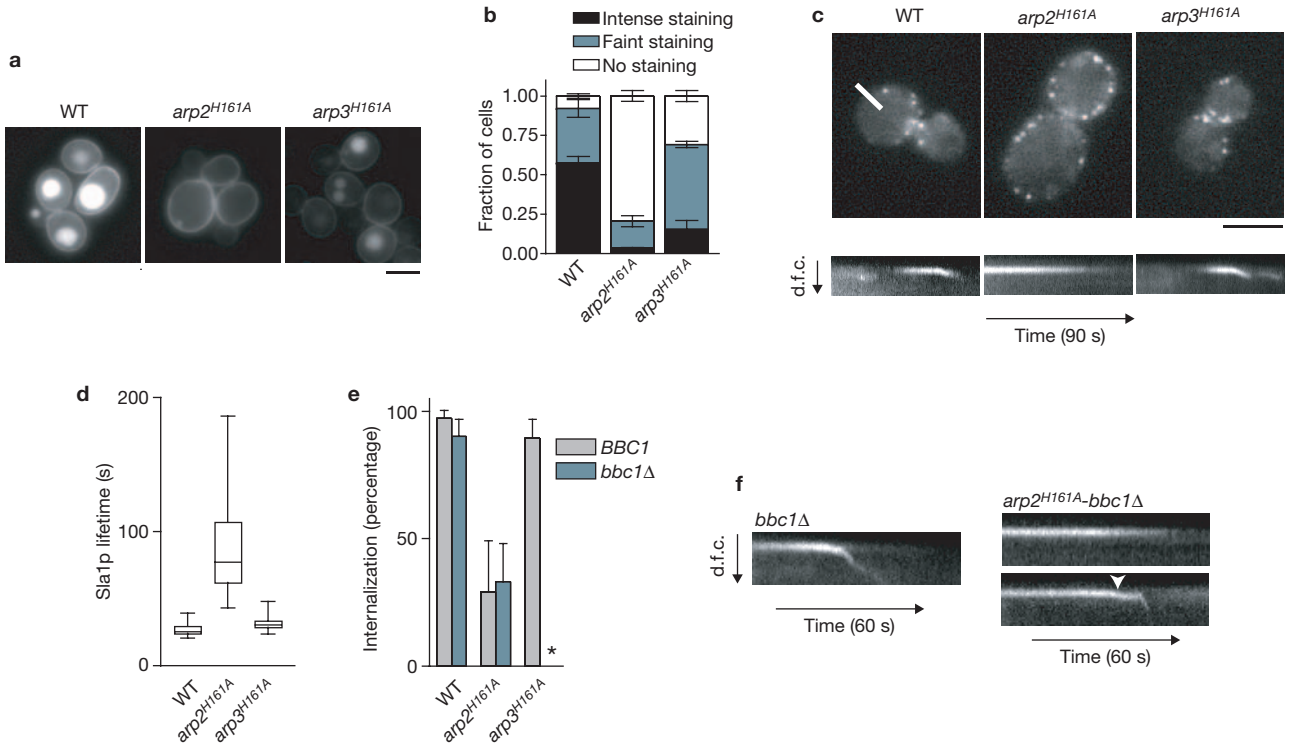

Figure 2 Arp2 ATP hydrolysis is required for productive endocytic internalization. (**a**) The *arp2*^{H161A} mutant is defective in endocytosis. Endocytic internalization of the fluid-phase marker, Lucifer yellow, was examined by fluorescence microscopy. (**b**) Quantification of Lucifer yellow internalization. The error bars represent mean ± s.d. (n = 3). Intense, faint and no staining were defined as 51–100%, 17–50% and 0–16% of the maximal Lucifer yellow fluorescence intensity, respectively. (**c**) The *arp2*^{H161A} mutant shows defects in the internalization of an endocytic adaptor, Sla1p. Single frames (top) and kymographs of single patches (bottom) from movies of wild-type and mutant cells expressing Sla1–GFP (2.8 frames per s). Kymographs were generated using a line perpendicular to the plasma membrane (that is, the white line in the top left panel). d.f.c.; distance from the cortex. (**d**) Sla1–GFP lifetime was calculated from 20 individual patches per strain. Data is represented by a 'box-and-whiskers' graph in which boxes extend from the 25th to the 75th percentile, with a line at the median. Whiskers extend to the most extreme values. (**e**) The percentage of Sla1–GFP patches that moved inward was calculated for at least 50 patches per strain. The error bars represent the mean ± s.d. (n = 3). The asterisk indicates that the *arp3*^{H161A}*-bbc1Δ* mutant was not examined. (**f**) The *arp2*^{H161A} mutant affects multiple steps of endocytic internalization. Sla1–GFP movement was examined in the *bbc1Δ* background. Images represent kymographs of single patches from movies of cells expressing the indicated mutants (2 frames per s). The arrowhead indicates the discontinuous Sla1–GFP inward movement observed in the *arp2*^{H161A} mutant. The scale bar represents 4 μm in **a** and **c**.

90 min, *arp2*^{H161A} cells showed a striking deficiency in uptake of Lucifer yellow (Fig. 2a, b). The *arp3*^{H161A} mutant showed an intermediate defect in Lucifer yellow uptake, further indicating that both of these mutants affect Arp2/3 complex function (Fig. 2a, b).

Actin and the Arp2/3 complex colocalize in budding yeast at dynamic cortical actin patches[11,12], which are endocytic sites[13–17]. Actin-patch assembly and internalization coincide with the slow inward movement of clathrin and endocytic adaptor proteins such as Sla1p[13,14,16]. Inward movement of Sla1p may reflect the invagination step of clathrin-coated vesicle formation and is driven by Arp2/3-mediated actin polymerization[6,13,14]. We therefore examined Sla1–GFP movement in the H161A mutants. The *arp2*^{H161A} mutant exhibited a threefold increase in Sla1–GFP cortical lifetime and a 70% reduction in the frequency of Sla1–GFP inward movements (Fig. 2c–e and see Supplementary Information, Movie 1), demonstrating that Arp2 ATP hydrolysis is crucial for endocytic internalization. The *arp3*^{H161A} mutant had a minor Sla1–GFP internalization defect (Fig. 2c–e and see Supplementary Information, Movie 1). Deletion of a negative regulator of Arp2/3-mediated nucleation, Bbc1p[18], has been shown to increase the speed and distance of Sla1–GFP movement[14]. Therefore, Sla1–GFP movement was examined in the *bbc1Δ* background to accentuate differences between wild-type and *arp2*^{H161A} cells. In *arp*^{H161A}*-bbc1Δ* cells, 70% of Sla1–GFP patches failed to internalize (Fig. 2e, f and see Supplementary Information, Movie 2). In addition, Sla1–GFP patches that were internalized in *arp*^{H161A}*-bbc1Δ* cells moved discontinuously, often pausing below the plasma membrane before continuing into the cytoplasm (Fig. 2f). This phenotype possibly indicated a secondary defect in vesicle scission and/or actin network release from the plasma membrane. Overall, these results demonstrate that Arp2 ATP hydrolysis is important for Arp2/3-mediated force generation *in vivo*, possibly functioning at multiple steps of endocytic vesicle formation.

To determine whether the *arp2*^{H161A} mutant affects actin assembly and/or disassembly at endocytic sites, endocytic actin dynamics were examined using Sac6p (yeast fimbrin), a marker for filamentous actin. In wild-type cells, Sac6p assembles at immotile Sla1p patches and the two proteins co-internalize[14]. The *arp2*^{H161A} mutant exhibited an 80% reduction in the frequency of Sac6–GFP internalization and the 'lifetime' of Sac6–GFP was threefold longer compared with wild-type cells (data not shown), consistent with its endocytic defect. Interestingly, *arp2*^{H161A} and *arp3*^{H161A} only slightly decreased the rate of Sac6p assembly at Sla1–GFP-containing patches (Fig. 3a, b and see Supplementary Information, Movie 3). However, *arp2*^{H161A} Sac6–GFP patches that

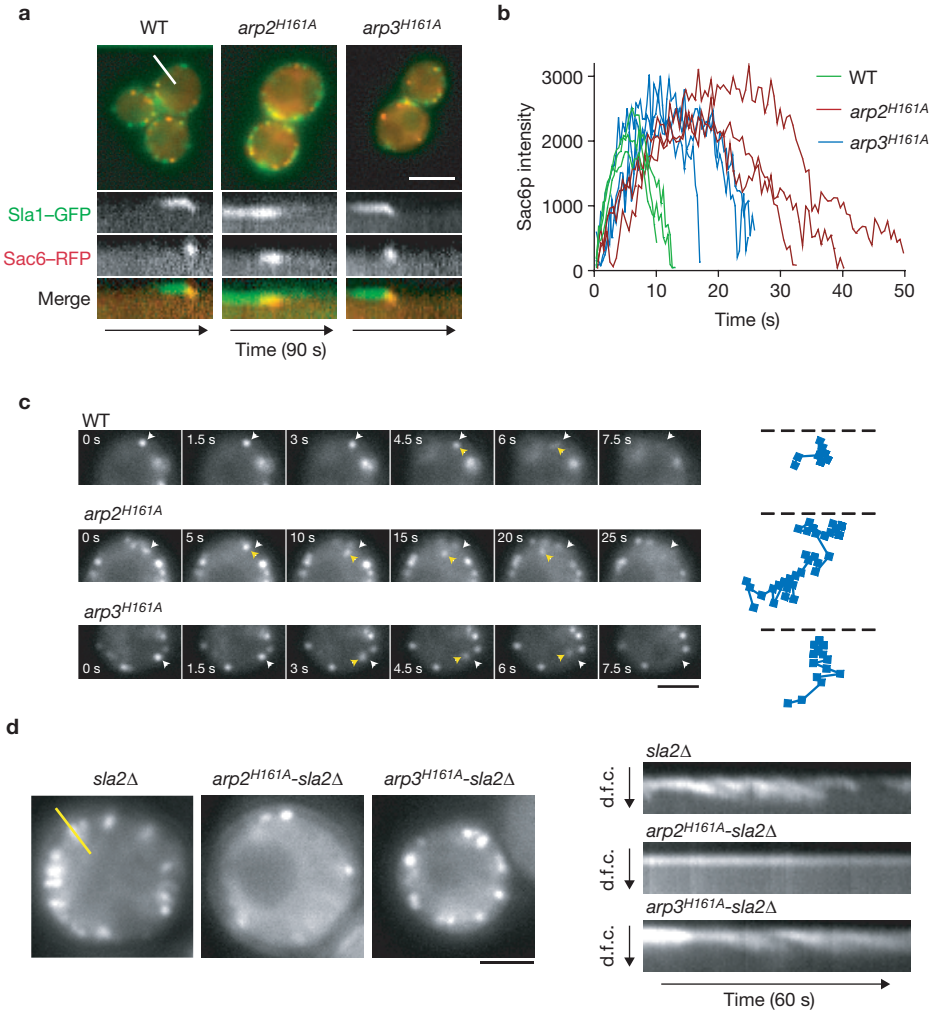

Figure 3 Arp2 ATP hydrolysis is required for proper actin network disassembly. (**a**) Actin assembly occurs at endocytic sites in the *arp2*^{H161A} mutant. Single frames (top) and kymographs of single patches (bottom) from movies (1 frame per s) of wild-type and mutant cells expressing Sla1–GFP and Sac6–RFP. Kymographs were generated using a line perpendicular to the plasma membrane (that is, the white line in top left panel). (**b**) Actin disassembly is delayed in the *arp2*^{H161A} mutant. Sac6–GFP patch intensity was calculated for individual patches from a movie with a time-lapse of 0.25 s. (**c**) Internalized Sac6–GFP patches exhibit increased lifetime in the *arp2*^{H161A} mutant. Time-lapse images of cells expressing Sac6–GFP and the indicated mutant (left). The white arrowheads indicate the starting position of the Sac6–GFP patch and the yellow arrowheads follow the moving patch. Note that the interval between frames is longer for *arp2*^{H161A} than for wild type and *arp3*^{H161A}. Tracks of individual Sac6–GFP patches are shown on the right. The time between data points is 0.5 s. (**d**) Arp2 ATP hydrolysis is required for actin network retrograde flow. Single frames (left) and kymographs of single tails (right) from movies of *sla2Δ* cells expressing Sac6–GFP to label actin (2 frames per s). Kymographs were generated using a line perpendicular to the plasma membrane (that is, the yellow line in the left panel). The scale bars represent 4 μm in **a** and 2 μm in **c** and **d**.

failed to internalize exhibited a pronounced delay in actin disassembly (Fig. 3a, b). In addition, internalized Sac6–GFP patches in *arp2*^{H161A} cells persisted in the cytoplasm for 12.6 ± 9.6 s (n = 20), compared with 4.0 ± 1.4 s (n = 20) in wild-type cells, before disassembling or moving out of the focal plane (Fig. 3c and see Supplementary Information, Movie 4). Sac6–GFP patches in the *arp2*^{H161A} mutant were sometimes seen to fuse, resulting in mobile cytoplasmic clumps with lifetimes >60 s (see Supplementary Information, Movie 5). It is most likely that the prolonged Sac6p lifetime resulted from an actin disassembly defect, rather than continued actin nucleation, because the plasma membrane associated NPFs, Las17p and Myo5p, remained associated with the plasma membrane during internalization (see Supplementary Information, Fig. S3a), and neither Las17p, Myo5p nor the NPF Pan1p localized to the long-lived Sac6–GFP-containing structures (data not shown). Furthermore, both *arp2*^{H161A} and *arp3*^{H161A} mutant actin patches and cell growth showed elevated resistance to the actin monomer-sequestering drug, latrunculin A (see Supplementary Information, Fig. S3b–d). Therefore, in addition to affecting endocytic internalization, both the Arp2 and Arp3 ATP hydrolysis mutants impede actin network disassembly.

As wild-type actin patches are smaller than the limits of resolution for light microscopy, mutants with exaggerated cortical actin structures are valuable tools for examining actin network organization and dynamics at yeast endocytic sites[6,13,14]. The *sla2Δ* mutant blocks endocytosis and causes the formation of elongated actin tails in which actin subunits continuously flow from an endocytic complex at the plasma membrane into the cytoplasm[13]. Phenotypic analysis of this mutant, and others, suggested that actin nucleation occurs near the plasma membrane and that retrograde movement of actin filaments tethered to endocytic coat proteins drives endocytic internalization[13,14]. To determine whether Arp2 ATP hydrolysis is required for actin tail formation,

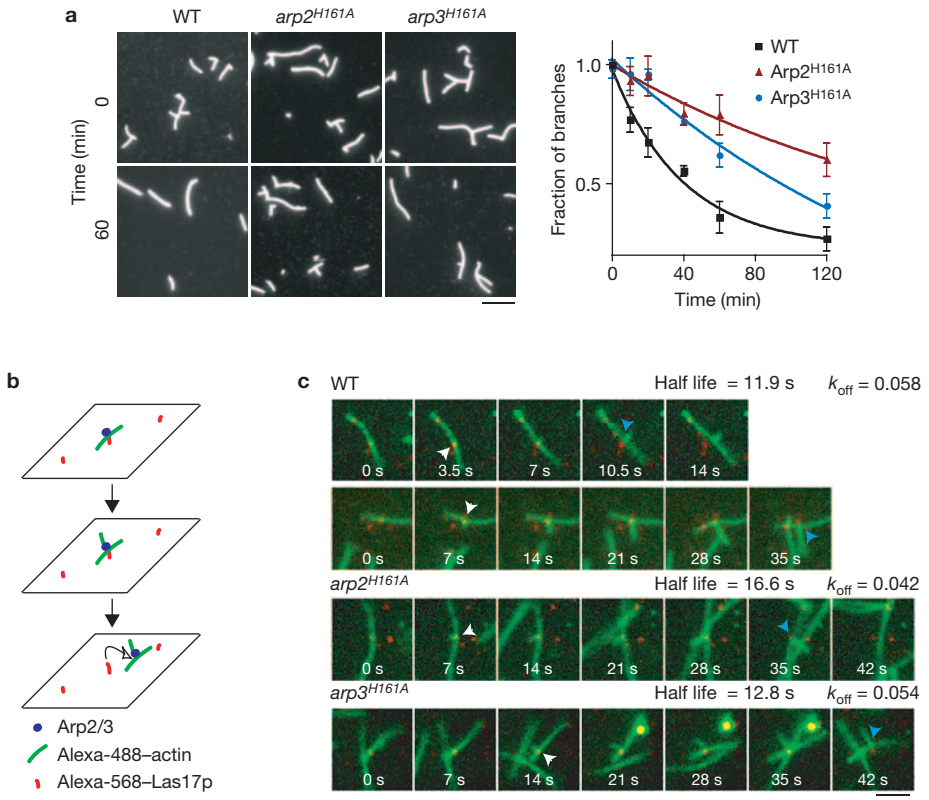

Figure 4 Arp2, and possibly Arp3, ATP hydrolysis is required for efficient y-branch dissociation. (**a**) Arp2/3 y-branches are more stable in the H161A mutants. Fluorescence micrographs of rhodamine–phalloidin labelled actin filaments (left) are shown either 0 or 60 min after steady-state levels of actin assembly were reached. The number of branches per μm of filament at different times were quantified and normalized to the starting branch frequency (right). Data points represent the mean ± s.d. ($n = 4$ for WT and Arp2^{H161A}, $n = 2$ for Arp3^{H161A}). (**b**) Schematic representation of the NPF release assay. The cartoon shows y-branch formation in association with a Las17p particle and subsequent y-branch release from Las17p. (**c**) The H161A mutants do not prevent NPF release. The montages represent images of individual branching events from a time-lapse movie (1 frame per 3.5 s). Alexa-488–actin was visualized by TIRF microscopy, whereas Alexa-568–Las17p was visualized by epifluorescence. The white arrowheads indicate the formation of a y-branch in association with Alexa-568–Las17p and the blue arrowheads indicate the y-branch after it has been released from Alexa-568–Las17p. The half-life and k_{off} were calculated by fitting the distribution of release events (see Supplementary Information, Fig. S4c) to a monoexponential curve. The scale bars represent 5 μm in **a** and 2 μm in **c**.

the actin networks in *arp2^{H161A}-sla2Δ* and *arp3^{H161A}-sla2Δ* double mutants were visualized using Sac6–GFP. Despite increasing nucleation activity *in vitro*, the *arp2^{H161A}* mutant suppressed actin tail formation in the *sla2Δ* mutant. Actin structures formed, but did not efficiently extend away from the plasma membrane in *arp2^{H161A}-sla2Δ* cells (Fig. 3d and see Supplementary Information, Movie 6). Other Arp2/3 mutants, including *arp3^{H161A}* (Fig. 3d), *arp3^{G302Y}* (ref. 6), *arp3^{D11A}* and *arp2^{D11A}* (data not shown), formed elongated actin tails when combined with *sla2*Δ. Therefore, *arp2^{H161A}* specifically impairs actin-network retrograde flow at endocytic sites.

Arp2 ATP hydrolysis may facilitate actin network disassembly *in vivo* by promoting y-branch dissociation[8]. To determine whether *arp2^{H161A}* affects y-branch stability, actin filaments from nucleation reactions were fixed with rhodamine–phalloidin at different times and visualized using fluorescence microscopy[8,19]. Y-branches nucleated by wild-type yeast Arp2/3 complex dissociated with a half-life of 27 min (Fig. 4a)[8,19]. This debranching rate was approximately 100-fold slower than the rate of Arp2 ATP hydrolysis. Despite this difference in rates, Arp2^{H161A} stabilized y-branches nucleated by the Arp2/3 complex, increasing their half-life to 126 min (Fig. 4a). Interestingly, Arp3^{H161A} also stabilized y-branches, suggesting the possibility that Arp3 might hydrolyse ATP (Fig. 4a). Increased branch stability was correlated with the *in vivo* effects of these mutants on endocytosis and actin disassembly (Fig. 2b). Because the *in vitro* debranching rate is >100-fold longer than actin-patch lifetime, it is likely that proteins such as cofilin accelerate debranching in cells[19]. Both *arp2^{H161A}* and *arp3^{H161A}* were synthetic lethal with *cof1-22*, a temperature sensitive cofilin mutant[20] (see Supplementary Information, Fig. S3e and Table S1). In addition, *arp2^{H161A}* was synthetic lethal with the *aip1Δ* mutant (see Supplementary Information, Table S1), which encodes a protein that interacts with cofilin to induce actin-filament disassembly[21]. Thus, Arp2/3 ATP hydrolysis and cofilin may cooperate to disassemble the actin meshwork.

It has been suggested that membrane-bound NPFs release Arp2/3-containing y-branches, thus allowing actin-filament elongation adjacent to a surface[22,23]. Impaired NPF release may stabilize y-branches *in vitro* and cause endocytic defects *in vivo*. Therefore, we directly visualized NPF release *in vitro* by immobilizing Alexa-568-labelled Las17p (Alexa-568–Las17p) on the surface of a coverslip and then observing actin polymerization using total internal reflection fluorescence (TIRF) microscopy (Fig. 4b and see Supplementary Information, Fig. S4a, b). Y-branches formed in association with Alexa-568–Las17p and were released from Alexa-568–Las17p within 20 s of the nucleation event, exhibiting an off rate of approximately 0.06 s (Fig. 4c and see Supplementary Information, Movie 7). This demonstrates that

Table 1 The *arp2*^{H161A} and *arp3*^{H161A} mutant phenotypes are not due to reduced actin nucleation

	arp3^{G302Y} (ts, ss, fs)	*arp2*^{H161A} (ss, fs)	*arp3*^{H161A} (WT)
las17-ΔA (WT)	Synthetic lethal	Suppression	No effect
pan1-KE101 (WT)	Synthetic sick	Suppression	Not determined
arp2^{Y306A} (WT)	Suppression		Synthetic sick / synthetic lethal
arp3^{F306A} (WT)	Synthetic sick / synthetic lethal		

The H161A mutants are distinct from mutants that decrease Arp2/3-complex nucleation activity. Synthetic phenotypes of double-mutant combinations between Arp2 and Arp3 mutants, and Arp2/3 and NPF mutants are shown. Genetic interactions were examined by analysing at least 12 tetrads from each cross and identifying double mutants using linked auxotrophic markers. The phenotypes of the starting single-mutant strains are indicated in brackets. A synthetic-lethal phenotype indicates that the resulting double-mutant spores were unable to grow at 25 °C. A synthetic-sick phenotype indicates that the double-mutant spores grew less well than either single mutant. ts, temperature sensitive; ss, salt sensitive; fs, formamide sensitive.

WASP-family proteins rapidly release y-branches after nucleation, consistent with conclusions from electron microscopy studies[24]. Importantly, Las17p released Arp2^{H161A} and Arp3^{H161A} y-branches similarly to wild type (Fig. 4c and see Supplementary Information, Fig. S4c and Movie 8). Thus, Arp2^{H161A} and Arp3^{H161A} branch stabilization is not due to failed NPF release.

Because Arp2^{H161A} and Arp3^{H161A} stabilized y-branches *in vitro*, their mutant phenotypes may result from a debranching defect, rather than an actin nucleation defect. If this hypothesis is true, then *arp2*^{H161A} genetic interactions should be distinct from those of the nucleation defective *arp3*^{G302Y} mutant[6]. Two mutants, *las17–ΔA* and *pan1-KE101*, encode NPFs defective in Arp2/3 binding[25,26] and are synthetic sick or lethal with *arp3*^{G302Y} (ref. 6). In contrast, *arp2*^{H161A} growth was partially suppressed by *las17–ΔA* and *pan1-KE101* (Table 1 and see Supplementary Information, Fig. S5a). NPF mutants possibly suppress *arp2*^{H161A} by lowering the number of hyper-stable y-branches nucleated at endocytic sites. Furthermore, both H161A mutants exhibited synthetic sickness or lethality with the Y(F)306A class of Arp2/3 mutants (Table 1 and see Supplementary Information, Fig. S5b), which increase nucleation activity *in vitro* and suppress growth defects of nucleation-defective mutants[6]. Therefore, *arp2*^{H161A} and *arp3*^{H161A} do not impair endocytosis by reducing actin nucleation at endocytic sites.

A summary of Arp2/3 hydrolysis mutant effects is presented in the Supplementary Information, Table S2. Previous studies suggested that Arp2 ATP hydrolysis is critical for actin nucleation[3,4]. Here, we used the *arp2*^{H161A} mutant to demonstrate that Arp2 ATP hydrolysis is not required for nucleation or NPF release, but is essential for efficient y-branch dissociation. The *arp3*^{H161A} mutant also delayed debranching *in vitro* and exhibited actin-disassembly defects *in vivo*. This result was unexpected because Arp3 ATP hydrolysis was not observed *in vitro*[7,8]. We speculate that the *arp3*^{H161A} phenotype results from a defect in Arp3 ATP hydrolysis, which may also promote debranching. Because ATP crosslinking may inactivate the ATP-hydrolysis activity of Arp3, new techniques are required to fully assess this activity. Arp2 and Arp3 have been shown to associate with the daughter-filament pointed end in y-branches, with Arp2 making the majority of contacts[24,27]. We propose that Arp2/3 ATP hydrolysis, predominantly by Arp2, mediates release of the daughter-filament pointed end, allowing actin filament reorganization and depolymerization (Fig. 5).

Arp2 ATP hydrolysis occurs within 20 s of nucleation, >100-fold faster than the debranching rate. Other factors, such as ADF–cofilin and/or mechanical load, are likely to cooperate with Arp2/3 ATP hydrolysis to accelerate debranching *in vivo*. The ADF–cofilin protein actophorin greatly accelerates debranching *in vitro*[19], possibly by increasing the rate of P_i release from actin filaments[28]. Our data suggest that Arp2/3 ATP hydrolysis and cofilin may cooperate to facilitate actin-network disassembly in cells. Importantly, the *arp2*^{H161A} single mutant delays actin-network disassembly, suggesting that cofilin-mediated actin-filament disassembly may require debranching.

Arp2/3 ATP hydrolysis is crucial for endocytic internalization. Suppression of *arp2*^{H161A} phenotypes by NPF loss-of-function mutants suggests that the *arp2*^{H161A} phenotype is not due to impaired actin nucleation that results indirectly from reduced actin turnover. This genetic interaction also suggests that the increased nucleation activity of *arp2*^{H161A} and *arp3*^{H161A} could enhance their mutant phenotypes. However, increased nucleation activity alone cannot explain the observed defects, because a mutant that similarly increases nucleation activity (*arp2*^{Y306A}) has no endocytic defect[6] or synthetic phenotype with *cof1-22* (data not shown). Therefore, debranching seems to be a distinct Arp2/3 complex activity that is required for endocytic internalization. We propose that debranching and subsequent actin network remodelling are required to accommodate the changing geometry of a budding endocytic vesicle (Fig. 5). In addition, remodelling may release endocytic vesicles and actin from the plasma membrane after scission. Endocytic proteins, such as mammalian cortactin, possibly regulate branch stability during endocytic internalization[29]. It is likely that the *arp2*^{H161A} mutant interferes with the spatial–temporal regulation of branch stability, resulting in an intractable actin network that presents a barrier to endocytic-coat and actin-network internalization (Fig. 5). Consistent with this hypothesis, *arp2*^{H161A} suppressed the actin-tail phenotype in *sla2Δ* cells, impeding actin-filament retrograde movement at endocytic sites. In summary, y-branch dynamics are a critical feature of actin networks that need to be explored to fully understand the functions of actin in endocytosis and cell motility. □

METHODS

Yeast strains and media. The yeast strains used in this study are listed in the Supplementary Information, Table S3. Arp2/3 mutants and GFP/RFP tagged proteins were generated as previously described[6,14]. All strains were grown in rich media at 25 °C unless otherwise noted.

ATP hydrolysis and nucleation assays. Yeast Arp2/3 complex, Las17p and rabbit skeletal muscle actin were purified as previously described[6,18]. Arp2/3 complex (1 μM) in KMEI buffer (50 mM KCl, 1 mM MgCl2, 1 mM EGTA, 10 mM imidazole at pH 7.0) was equilibrated with 8-azido-γ-^{32}P-ATP (6 μM; Affinity Labeling Technologies, Inc., Lexington, KY) for 2 min and irradiated with 254 nm UV light for 10 s using a hand-held Mineralight lamp. The crosslinking reaction was stopped with 1 mM ATP and 1 mM DTT. γ-^{32}P-ATP-labelled Arp2/3 complex (10 nM) was mixed with actin (2 μM) and polymerization buffer (final concentration: 50 mM KCl, 1 mM MgCl2, 1 mM EGTA). An aliquot was removed for the 0 min time point and Las17p was then added (50 nM) to initiate the reaction. Aliquots (400 μl) were removed at different times and mixed with 80% methanol : 20% chloroform (500 μl) to precipitate the proteins. Samples were subjected to SDS–PAGE and analysed using a Typhoon 9400 Phosphoimager (GE Healthcare, Piscataway, NJ).

To measure Arp2/3-mediated actin assembly, pyrene fluorescence was monitored. Actin (2 μM, 5% pyrene-labelled) was mixed with the indicated proteins

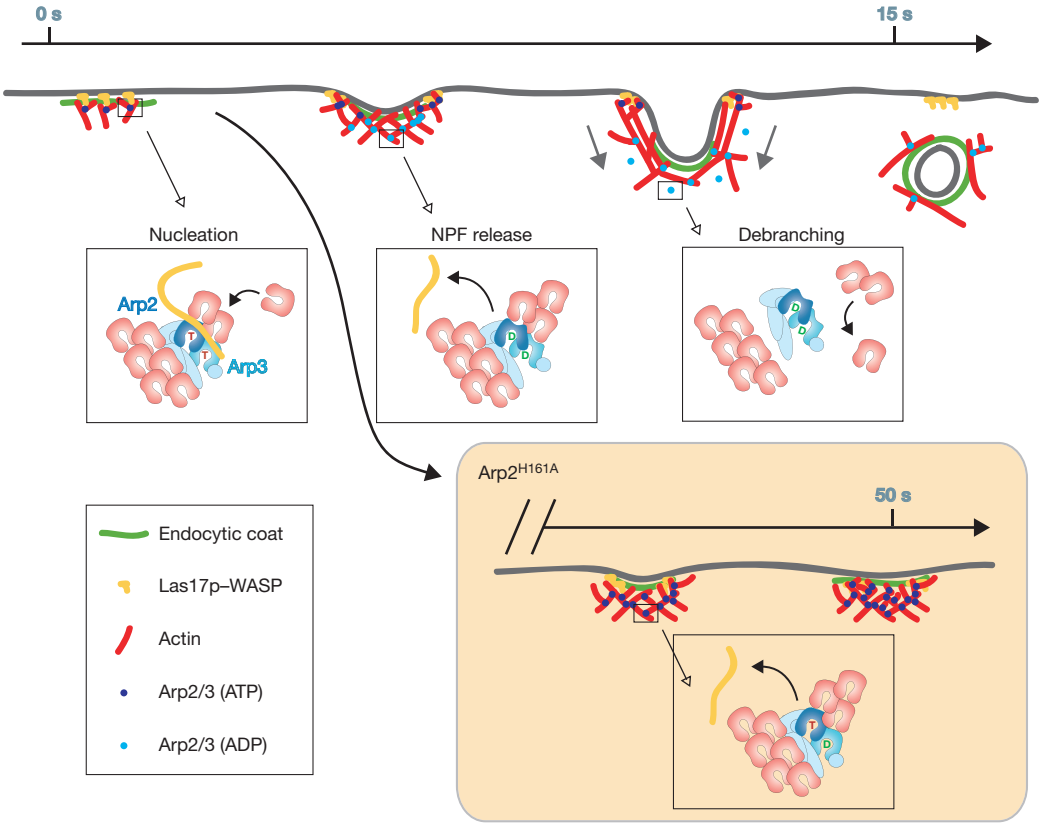

Figure 5 Schematic representation of a model for Arp2/3 complex ATP hydrolysis function. Las17p and other NPFs activate the Arp2/3 complex at endocytic sites, generating actin y-branches. Y-branches are released from membrane-bound NPFs and Arp2 ATP hydrolysis destabilizes the branch. Other proteins, such as cofilin, may accelerate branch dissociation or debranching. Debranching allows actin network remodelling around the emerging endocytic vesicle and eventual actin-network disassembly. In the *arp2*^{H161A} mutant, branches are stabilized, preventing y-branch reorganization and endocytic internalization.

and added to a cuvette containing polymerization buffer. Fluorescence data were collected using a Fluoromax 3 fluorometer (Jobin-Yvon Horiba, Edison, NJ). To relate nucleation activity to Arp2 ATP hydrolysis (Fig. 1e), identical reagents were used (with the exception of γ-^{32}P-ATP-labelled Arp2/3) to perform both the actin assembly and ATP hydrolysis assays. Free barbed-end concentrations nucleated by the Arp2/3 complex were calculated by first fitting the experimental data to a model of autocatalytic actin assembly[30] and then calculating barbed-end concentrations using a rate constant of 8.7 $\mu M^{-1}\,s^{-1}$, as previously described[6]. To calculate the concentrations of ATP hydrolysed, the initial γ-^{32}P-ATP-labelled Arp2 intensity was scaled to the total amount of Arp2/3 complex (10 nM). The amount of Arp2 hydrolysis was determined by the decrease in the ^{32}P signal (Fig. 1c). 8-azido-ATP crosslinking did not affect Arp2/3 complex nucleation (data not shown). We assumed that non-crosslinked Arp2 hydrolyses ATP at the same rate as crosslinked ATP.

Microscopy. For live-cell imaging, strains were grown at 25 °C to $A_{60} = 0.1–0.5$ in minimal media lacking tryptophan (SD–Trp) and adhered to the surface of a Con A-coated coverslip. To create a chamber, a coverslip was inverted onto a glass slide containing a square outline of vacuum grease and the sample was imaged at room temperature. Single-colour movies were obtained using an Olympus IX-81 microscope, 100× NA 1.4 objective and an Orca-ER camera (Hamamatsu, Hamamatsu City, Japan). Two-colour movies were obtained by switching between RFP and GFP filter sets. All image processing was performed using ImageJ (http://rsb.info.nih.gov/ij/) as previously described[13].

Debranching assay. Actin (2 μM, 5% pyrene-labelled) was polymerized with Arp2/3 complex (50 nM) and Las17p WCA (500 nM). To compensate for the higher nucleation activity of the H161A mutants, a fivefold lower concentration of Arp2/3 complex (10 nM) was used to ensure that the nucleation activity and starting-branch density was equivalent to that of 50 nM wild-type Arp2/3 complex. Aliquots were removed at different times and stabilized with rhodamine–phalloidin to visualize actin filaments. The first time point was taken after steady-state levels of actin polymer were reached. Rhodamine–phalloidin-stabilized actin filaments were processed for imaging as previously described[6]. Branch density was calculated by counting branches manually and then using Fovea Pro 3.0 (Reindeer Graphics, Inc., Asheville, NC) for Adobe Photoshop 7.0 (Adobe Systems, Inc., San Jose, CA) to calculate total filament length. At least 8,000 μm of filaments were analysed for each time point.

NPF release assay. Monomeric actin was labelled at 4 °C for 4 h with a fivefold excess of Alexa-488–maleimide (GE Healthcare). DTT (2 mM) was added to stop the reaction and Alexa-488-labelled actin was gel filtered using a Superose 6 (Invitrogen, Carlsbad, CA) column to remove free dye. Las17p was dialysed into HE buffer (20 mM HEPES at pH 7.5, 1 mM EDTA) containing 0.5 M KCl (to prevent Las17p aggregation) and labelled for 12 h at 4 °C with Alexa-568–maleimide (Molecular Probes). Although actin that copurified with Las17p was also labelled with Alexa-568 (see Supplementary Information, Fig. S4a), it was unlikely to interfere with NPF-release measurements because actin alone is unable to form y-branches and Alexa-488–actin was present in >1,000-fold excess in the NPF-release assay. Alexa-568–Las17p alone adhered to glass coverslips. Therefore, to immobilize Las17p on the coverslip surface, Alexa-568–Las17p (0.5 nM) was incubated for 5 min in a flow chamber created using two pieces of double sided tape as spacers between a glass slide and a coverslip. Buffer was flowed through the chamber to remove unbound Alexa-568–Las17p and free dye. The chamber was subsequently blocked with 0.5% BSA. Alexa-568–Las17p single molecules (see Supplementary Information, Fig. S4b) or clusters could be detected by epifluorescence microscopy. Actin polymerization was initiated by adding actin (2 μM, 35% Alexa-488-labelled) and Arp2/3 complex (1–10 nM) to the flow chamber. The final reaction buffer was KMEI containing 3 mg ml^{-1} glucose, 0.1 mg ml^{-1} glucose oxidase, 20 μg ml^{-1} catalase, 10 mM DTT and 0.25% methylcellulose. Alexa-488–actin and Alexa-568–Las17p were imaged by alternating between TIRF and epifluorescence microscopy using an Olympus IX-81 microscope equipped with a

100× NA 1.45 objective. An argon-ion laser (Melles Griot, Carlsbad, CA) directed through the objective was used for TIRF microscopy. The observed interaction between Alexa-568–Las17p and y-branches was specific because y-branch formation was Arp2/3- and Las17p-dependent, and the addition of a tenfold excess of unlabelled Las17p to the reaction reduced the frequency of y-branches associated with Alexa-568–Las17p from 86% (n = 57) to 17% (n = 53).

Note: Supplementary Information is available on the Nature Cell Biology website.

ACKNOWLEDGEMENTS

We are very grateful to C. Toret and M. Kaksonen for providing yeast strains used in this study, P. Carlton for help with the calculation of branching frequency, and to S. Almo for helpful suggestions about potentially informative Arp2/3 mutations. In addition, we thank E. Goley, M. Kaksonen, V. Okreglak, C. Toret, Y. Sun, J. Wong, B. Pauly and A. Engqvist-Goldstein for their comments on the manuscript. Finally, we thank members of both the Drubin and Welch labs for their technical help and encouragement. This work was supported by National Institute of Health (NIH) grants GM42759 and GM50399 to D.G.D. and NIH grant GM59609 to M.D.W.

COMPETING FINANCIAL INTERESTS

The authors declare that they have no competing financial interests.

Published online at http://www.nature.com/naturecellbiology/
Reprints and permissions information is available online at http://npg.nature.com/reprintsandpermissions/

1. Pantaloni, D., Le Clainche, C. & Carlier, M. F. Mechanism of actin-based motility. *Science* **292,** 1502–1506 (2001).
2. Pollard, T. D. & Borisy, G. G. Cellular motility driven by assembly and disassembly of actin filaments. *Cell* **112,** 453–465 (2003).
3. Dayel, M. J., Holleran, E. A. & Mullins, R. D. Arp2/3 complex requires hydrolyzable ATP for nucleation of new actin filaments. *Proc. Natl Acad. Sci. USA* **98,** 14871–14876 (2001).
4. Le Clainche, C., Didry, D., Carlier, M. F. & Pantaloni, D. Activation of Arp2/3 complex by Wiskott-Aldrich Syndrome protein is linked to enhanced binding of ATP to Arp2. *J. Biol. Chem.* **276,** 46689–46692 (2001).
5. Goley, E. D., Rodenbusch, S. E., Martin, A. C. & Welch, M. D. Critical conformational changes in the Arp2/3 complex are induced by nucleotide and nucleation promoting factor. *Mol. Cell* **16,** 269–279 (2004).
6. Martin, A. C. *et al.* Effects of Arp2 and Arp3 nucleotide-binding pocket mutations on Arp2/3 complex function. *J. Cell Biol.* **168,** 315–328 (2005).
7. Dayel, M. J. & Mullins, R. D. Activation of Arp2/3 complex: addition of the first subunit of the new filament by a WASP protein triggers rapid ATP hydrolysis on Arp2. *PLoS Biol* **2**, E91 (2004).
8. Le Clainche, C., Pantaloni, D. & Carlier, M. F. ATP hydrolysis on actin-related protein 2/3 complex causes debranching of dendritic actin arrays. *Proc. Natl Acad. Sci. USA* **100,** 6337–6342 (2003).
9. Vorobiev, S. *et al.* The structure of nonvertebrate actin: implications for the ATP hydrolytic mechanism. *Proc. Natl Acad. Sci. USA* **100,** 5760–5765 (2003).
10. Moreau, V., Galan, J. M., Devilliers, G., Haguenauer-Tsapis, R. & Winsor, B. The yeast actin-related protein Arp2p is required for the internalization step of endocytosis. *Mol. Biol. Cell* **8,** 1361–1375 (1997).
11. Moreau, V., Madania, A., Martin, R. P. & Winsor, B. The *Saccharomyces cerevisiae* actin-related protein Arp2 is involved in the actin cytoskeleton. *J. Cell Biol.* **134,** 117–132 (1996).
12. Winter, D., Podtelejnikov, A. V., Mann, M. & Li, R. The complex containing actin-related proteins Arp2 and Arp3 is required for the motility and integrity of yeast actin patches. *Curr. Biol.* **7,** 519–529 (1997).
13. Kaksonen, M., Sun, Y. & Drubin, D. G. A pathway for association of receptors, adaptors, and actin during endocytic internalization. *Cell* **115,** 475–487 (2003).
14. Kaksonen, M., Toret, C. P. & Drubin, D. G. A modular design for the clathrin- and actin-mediated endocytosis machinery. *Cell* **123,** 305–320 (2005).
15. Huckaba, T. M., Gay, A. C., Pantalena, L. F., Yang, H. C. & Pon, L. A. Live cell imaging of the assembly, disassembly, and actin cable-dependent movement of endosomes and actin patches in the budding yeast, *Saccharomyces cerevisiae*. *J. Cell Biol.* **167,** 519–530 (2004).
16. Newpher, T. M., Smith, R. P., Lemmon, V. & Lemmon, S. K. *In vivo* dynamics of clathrin and its adaptor-dependent recruitment to the actin-based endocytic machinery in yeast. *Dev. Cell* **9,** 87–98 (2005).
17. Toshima, J. Y. *et al.* Spatial dynamics of receptor-mediated endocytic trafficking in budding yeast revealed by using fluorescent α-factor derivatives. *Proc. Natl Acad. Sci. USA* **103,** 5793–5798 (2006).
18. Rodal, A. A., Manning, A. L., Goode, B. L. & Drubin, D. G. Negative regulation of yeast WASp by two SH3 domain-containing proteins. *Curr. Biol.* **13,** 1000–1008 (2003).
19. Blanchoin, L., Pollard, T. D. & Mullins, R. D. Interactions of ADF/cofilin, Arp2/3 complex, capping protein and profilin in remodeling of branched actin filament networks. *Curr. Biol.* **10,** 1273–1282 (2000).
20. Lappalainen, P. & Drubin, D. G. Cofilin promotes rapid actin filament turnover *in vivo*. *Nature* **388,** 78–82 (1997).
21. Rodal, A. A., Tetreault, J. W., Lappalainen, P., Drubin, D. G. & Amberg, D. C. Aip1p interacts with cofilin to disassemble actin filaments. *J. Cell Biol.* **145,** 1251–1264 (1999).
22. Welch, M. D., Iwamatsu, A. & Mitchison, T. J. Actin polymerization is induced by Arp2/3 protein complex at the surface of *Listeria monocytogenes*. *Nature* **385,** 265–269 (1997).
23. Samarin, S. *et al.* How VASP enhances actin-based motility. *J. Cell Biol.* **163,** 131–142 (2003).
24. Egile, C. *et al.* Mechanism of filament nucleation and branch stability revealed by the structure of the Arp2/3 complex at actin branch junctions. *PLoS Biol.* **3**, E383 (2005).
25. Toshima, J., Toshima, J. Y., Martin, A. C. & Drubin, D. G. Phosphoregulation of Arp2/3-dependent actin assembly during receptor-mediated endocytosis. *Nature Cell Biol.* **7,** 246–254 (2005).
26. Duncan, M. C., Cope, M. J., Goode, B. L., Wendland, B. & Drubin, D. G. Yeast Eps15-like endocytic protein, Pan1p, activates the Arp2/3 complex. *Nature Cell Biol.* **3,** 687–690 (2001).
27. Volkmann, N. *et al.* Structure of Arp2/3 complex in its activated state and in actin filament branch junctions. *Science* **293,** 2456–2459 (2001).
28. Blanchoin, L. & Pollard, T. D. Mechanism of interaction of *Acanthamoeba* actophorin (ADF/Cofilin) with actin filaments. *J. Biol. Chem.* **274,** 15538–15546 (1999).
29. Weaver, A. M. *et al.* Cortactin promotes and stabilizes Arp2/3-induced actin filament network formation. *Curr. Biol.* **11,** 370–374 (2001).
30. Pantaloni, D., Boujemaa, R., Didry, D., Gounon, P. & Carlier, M. F. The Arp2/3 complex branches filament barbed ends: functional antagonism with capping proteins. *Nature Cell Biol.* **2,** 385–391 (2000).

nature cell biology

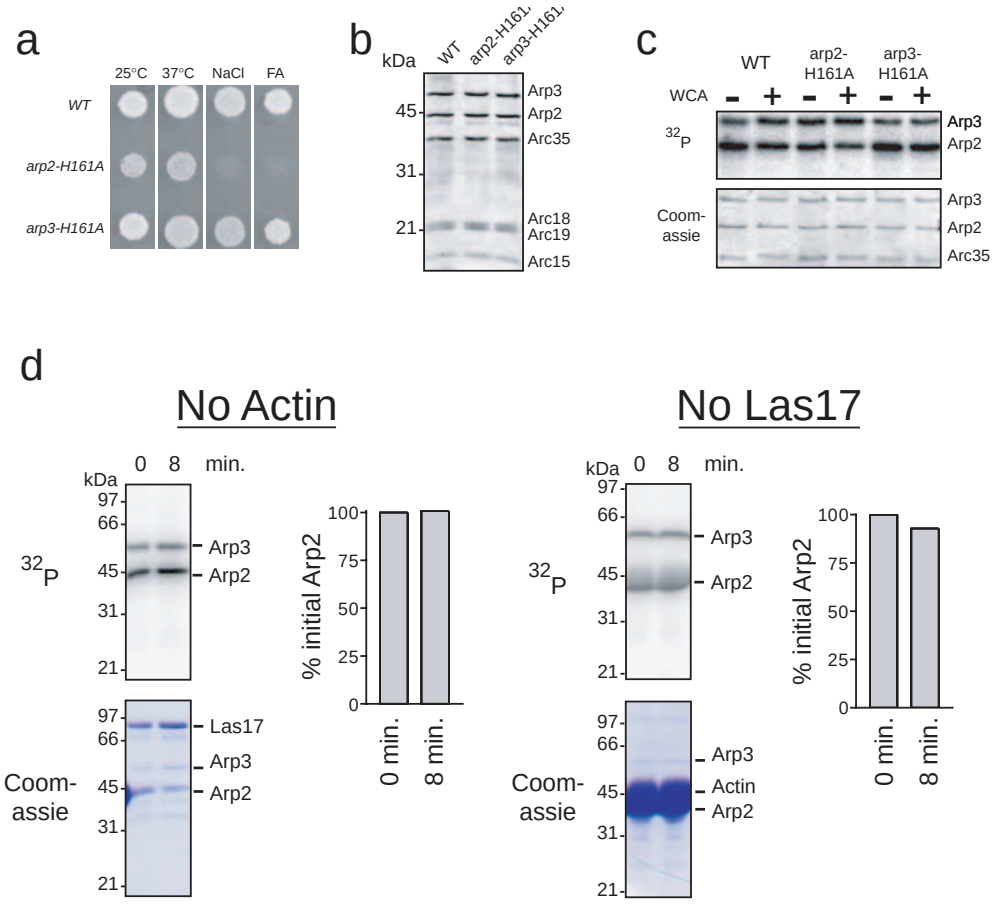

Figure S1 The *H161A* mutants are not significantly defective in ATP binding. **(a)** Growth phenotypes of the *H161A* mutants. NaCl and FA indicate rich media containing 0.9 M NaCl and 3% formamide, respectively. Strains were grown at 25 °C unless otherwise noted. **(b)** Coomassie blue stained gel of purified *H161A* mutant Arp2/3 complexes. **(c)** *H161A* mutants bind to ATP. Arp2/3 complexes (0.35 μM) with or without Las17p WCA (10 μM) were cross-linked to ATP (5 μM) spiked with α-[^{32}P]ATP for 5 min as described previously (Martin et al. 2005). Arp2/3 complex subunits were separated by SDS-PAGE and visualized by autoradiography (top) or Coomassie blue staining (bottom). **(d)** Arp2 ATP hydrolysis requires actin and Las17p. The Arp2/3 ATP hydrolysis assay was performed as described in Fig. 1a, except either actin (left) or Las17p (right) was not added. Bar graphs represent Arp2 ^{32}P signal normalized to the 0 min time point.

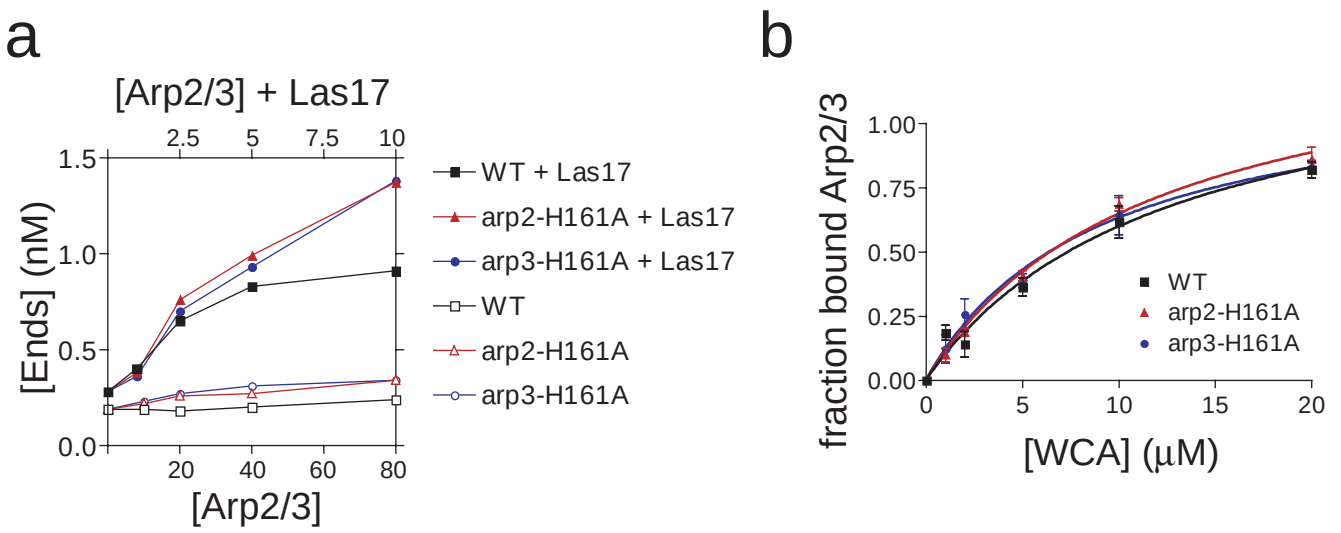

Figure S2 The *H161A* mutants do not impair Arp2/3 complex actin nucleation. **(a)** Nucleation activity of the *H161A* mutants. Barbed end concentrations were calculated at 50% polymerization using $k_+ = 8.7\ \mu M^{-1}\ s^{-1}$ (Higgs et al. 1999). The concentration of Arp2/3 complex was varied in the absence (open symbols, lower axis) and the presence (closed symbols, upper axis) of Las17p (10 nM). **(b)** Binding affinity of the *H161A* mutants to Las17p WCA. Increasing amounts of Las17p WCA-coated beads were added to Arp2/3 (80 nM) and loss of Arp3 from the supernatent was measured by Western blotting. K_d values of 12.4±1.3 μM, 11.7±1.7 μM, and 9±1.2 μM were calculated for wild-type, Arp2-H161A, and Arp3-H161A complexes.

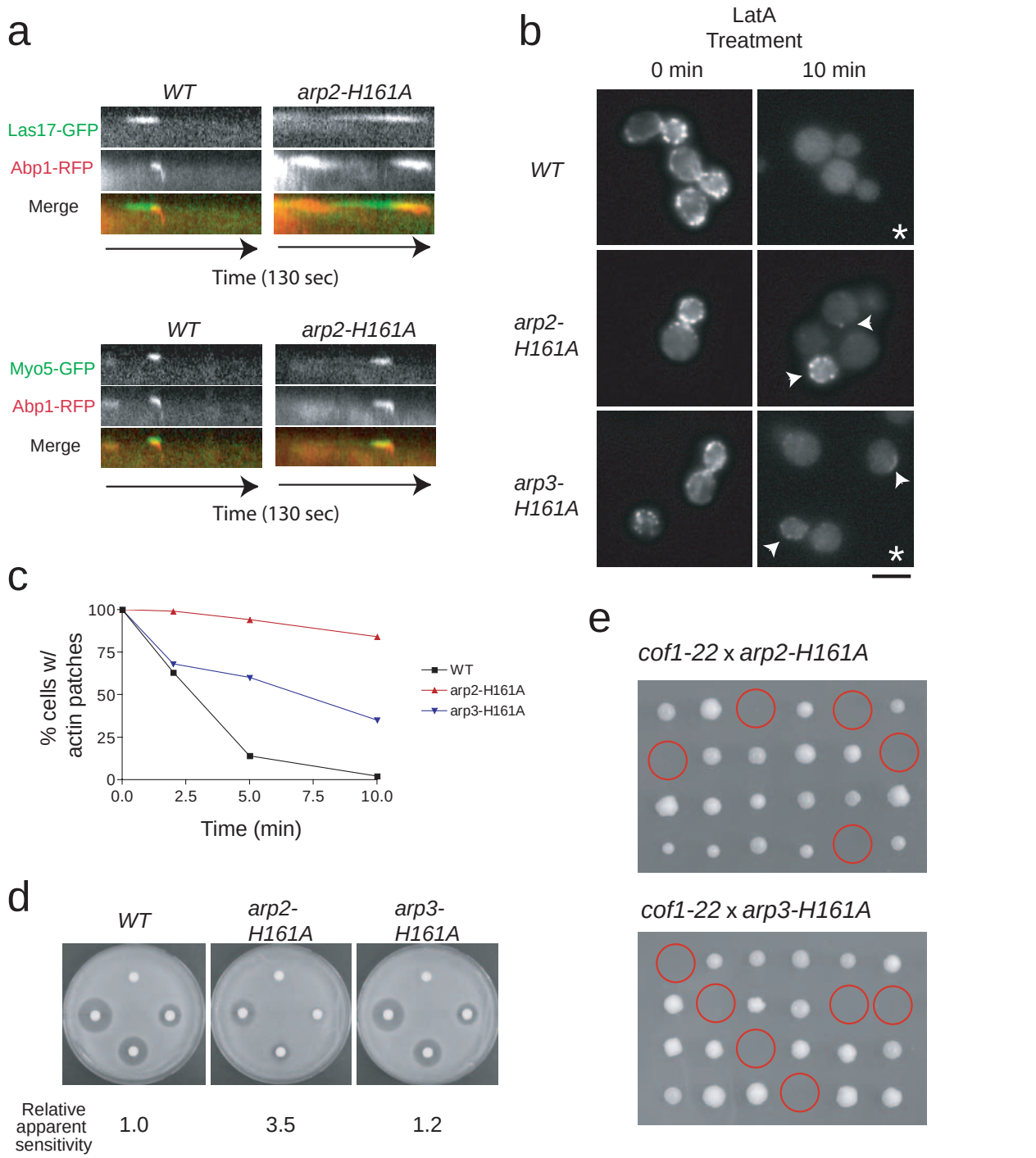

Figure S3 The *arp2-H161A* and *arp3-H161A* mutants show slower rates of actin patch disassembly. **(a)** Increased actin patch lifetime in the *arp2-H161A* mutant is not due to continued actin assembly. Kymographs of single patches from movies of cells expressing Abp1-RFP (a marker for actin) and either Las17-GFP or Myo5-GFP (1 frame/s). Note that Las17p and Myo5p remain associated with the plasma membrane in both wild-type and mutant cells. (b,c) Latrunculin A-induced depolymerization is slower in the *H161A* mutants than in wild-type cells. Cells (O.D. ~0.2) were treated with Latrunculin A (400 µM) for the indicated times, were fixed, and were then stained with rhodamine-phalloidin to label filamentous actin. Individual images of rhodamine-phalloidin stained cells are shown in **(b)**. Arrowheads indicate actin patches that remained after Latrunculin A treatment. Asterisks indicate frames in which the image brightness was increased relative to the other frames in order to reveal the absence or presence of actin patches. Scale bar = 4 µm. Quantification of the percentage of cells with visible actin patches, using 100 cells per time point, is shown in **(c)**. **(d)** *H161A* mutants show increased resistance to Latrunculin A. Halo assays were performed using 0, 0.5, 1, and 2 mM Latrunculin A, beginning at the top and moving in a clockwise direction. Relative apparent sensitivity is the fold increase in drug concentration required to achieve a halo diameter equivalent to that of wild-type. The slightly increased resistance of *arp3-H161A* was reproducible. **(e)** The *H161A* mutants exhibit synthetic lethality with a cofilin mutant. Tetrads resulting from a cross between the indicated mutants are shown. Red circles indicate double mutants.

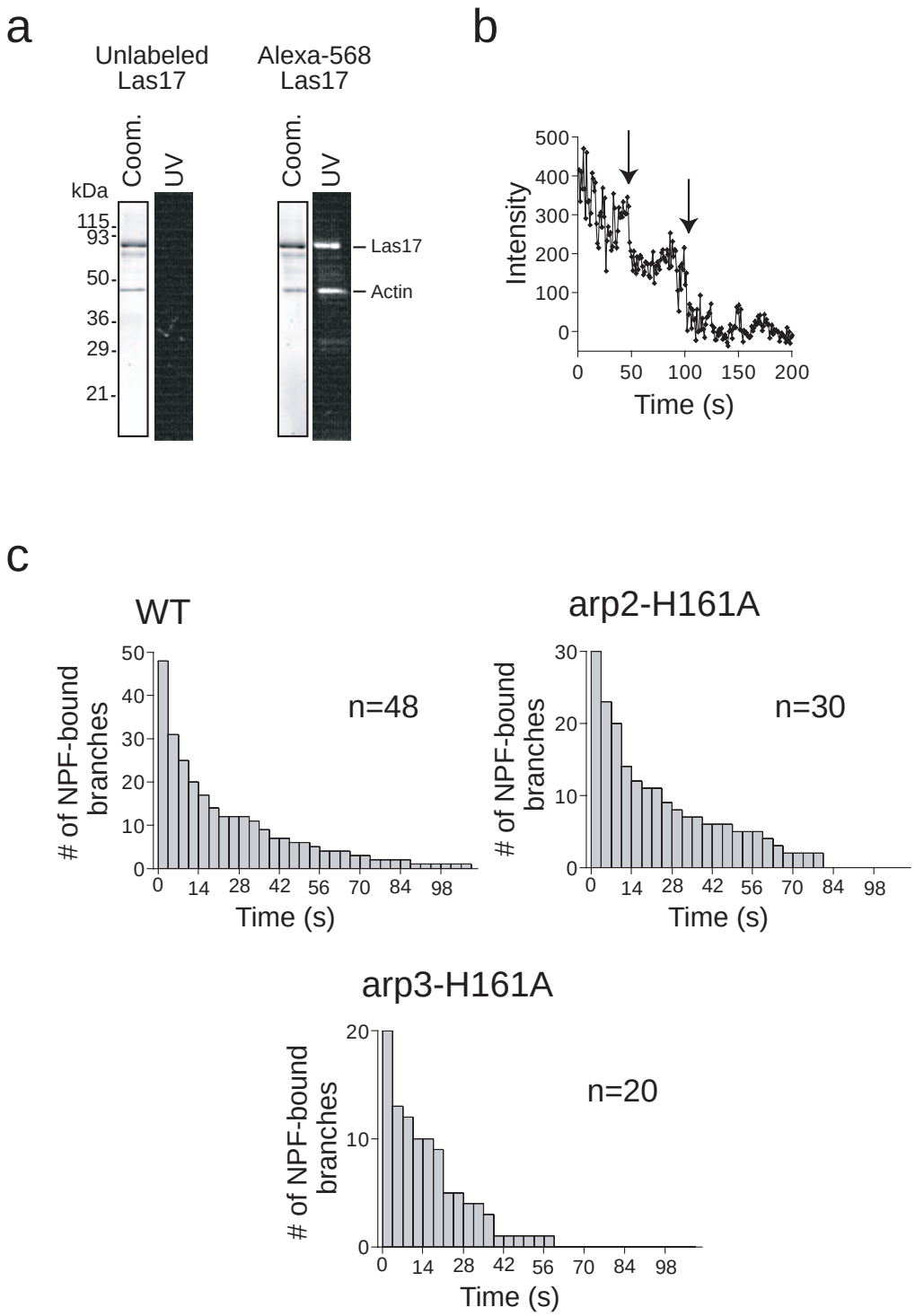

Figure S4 Visualizing Las17p's dynamic association with y-branches. **(a)** Labeling of Las17p with Alexa-568 dye. Unlabeled or labeled Las17p was visualized by Coomassie blue stain (left) or UV illumination (right). Actin, which copurified with Las17p, was also labeled with Alexa-568. **(b)** Single molecules of an Alexa-568-Las17p/Alexa-568-actin complex can be detected in the NPF release assay. A coverslip coated with Alexa-568-Las17p/actin was visualized with high lamp intensity. Data represents fluorescence intensity from a single Alexa-568-Las17p/actin spot. The two-step photobleaching suggests this spot represents a single Las17p/actin complex. For Fig. 4c, we show Alexa-568-Las17p/actin clusters, which are more easily visualized and similarly released y-branches. **(c)** The *H161A* mutants do not prevent NPF release. Data represents the number of y-branches that remained associated with Las17p for the indicated times. The average time of NPF release ± SD is 20.9 ± 28.1 s, 23.3 ± 24.2 s, and 17.7 ± 15.7 s for wild-type, Arp2-H161A, and Arp3-H161A Arp2/3 complexes, respectively. Half-lives calculated by fitting the data to a monoexponential decay curve are 11.9 s, 16.6 s, and 12.8 s for wild-type, Arp2-H161A, and Arp3-H161A, respectively.

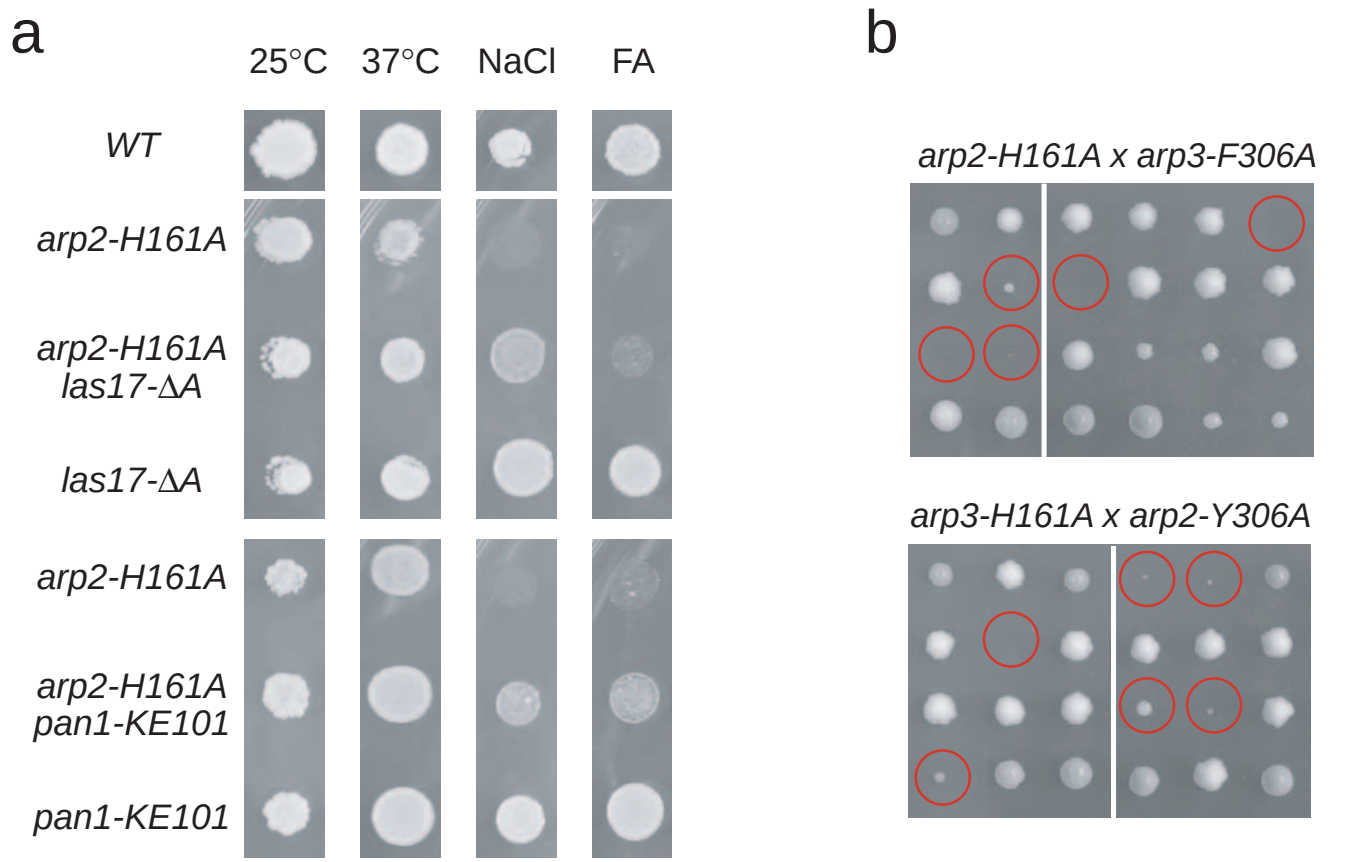

Figure S5 The *arp2-H161A* and *arp3-H161A* mutant phenotypes are not a result of reduced actin nucleation. **(a)** NPF loss-of-function mutants suppress the *arp2-H161A* mutant. NaCl and FA indicate rich media containing 0.9 M NaCl and 3% formamide, respectively. Strains were grown at 25 °C unless otherwise noted. **(b)** The *H161A* mutants are synthetic lethal with mutants that increase Arp2/3 activity. Tetrads resulting from a cross between the indicated mutants are shown. Red circles indicate double mutants.

Supplemental Video Legends

Video 1 Sla1-GFP internalization. Interval between frames is 0.36 s. The total time of image acquisition was 90 s.
Video 2 Sla1-GFP internalization in *bbc1*Δ cells. Interval between frames is 0.5 s. The total time of image acquisition was 60 s.
Video 3 Sac6-RFP (actin) and Sla1-GFP two-color movies. Sac6-RFP is red and Sla1-GFP is green. Interval between frames is 1.5 s. The total time of image acquisition was 90 s.
Video 4 Sac6-GFP (actin) internalization. Interval between frames is 0.5 s. The total time of image acquisition was 60 s.
Video 5 Sac6-GFP (actin) clumps in the *arp2-H161A* mutant. Left image represents a medial focal plane while the right image is focused near the cell surface. Interval between frames is 0.5 s. The total time of image acquisition was 60 s.
Video 6 Sac6-GFP (actin) tails in the *sla2*Δ mutant. Interval between frames is 0.5 s. The total time of image acquisition was 60 s.
Video 7 NPF release from Arp2/3 y-branches. Alexa-568-Las17p (red) was visualized using epifluorescence microscopy and Alexa-488-actin (green) was visualized using Total Internal Reflection Fluorescence (TIRF) microscopy. Interval between frames is 3.5 s. The total time of image acquisition was 210 s.
Video 8 NPF release from *H161A* mutant Arp2/3 y-branches. Alexa-568-Las17p (red) was visualized using epifluorescence microscopy and Alexa-488-actin (green) was visualized using Total Internal Reflection Fluorescence (TIRF) microscopy. The left panel is from an assay using Arp2-H161A Arp2/3 complex and the right panel is from an assay using Arp3-H161A Arp2/3 complex. Interval between frames is 3.5 s. The total time of image acquisition was 210 s.

Table S1. The *H161A* mutants exhibit specific synthetic lethal interactions with the *cof1-22* and *aip1*Δ mutants.

	cof1-22 *[ts,ss,fs]*	*aip1*Δ *[WT]*
arp2-H161A *[ss,fs]*	synthetic lethal	synthetic lethal
arp3-H161A *[WT]*	synthetic lethal	synthetic sick ts (34°C), ss, fs
arp3-G302Y *[ts,ss,fs]*	synthetic sick ts(34°C)	no interaction
arp3-D11A *[ts,ss,fs]*	synthetic sick ts(34°C)	

Synthetic phenotypes of double mutant combinations are indicated. Note that synthetic lethality with *cof1-22* is specific to the *H161A* mutants because two mutants that severely impair endocytosis, *arp3-G302Y* and *arp3-D11A*, only mildly enhance the *cof1-22* growth phenotype. Genetic interactions were examined by analyzing at least 10 tetrads from each cross and identifying double mutants using linked auxotrophic markers. The phenotypes of the single mutant strains are shown in brackets. A synthetic lethal phenotype means that double mutant spores were unable to grow at 25°C. A synthetic sick phenotype means that double mutants grew less well than either single mutant, resulting in the indicated growth phenotype. WT, wild-type; ts, temperature sensitive at 37°C unless otherwise noted; ss, salt sensitive; fs, formamide sensitive.

Table S2. Summary of *H161A* mutant phenotypes

Allele	Growth	Arp2 ATP hydrolysis	Nucleation activity	NPF release	Debranching	Lucifer yellow internalization	Sla1p internalization	Actin disassembly	*sla2*Δ tail formation
WT	**+** *wt*	**+** 5.8 nM	**+** 5.9 nM	**+** 11.9 s	**+** 27 min 0.23	**+** 91 %	**+** 97 %	**+** 4 s	**+**
arp2-H161A	**+/-** *ss, fs*	**-** 0.01 nM	**++** 7.5 nM	**+** 16.6 s	**-** 126 min 0.18	**-** 21 %	**-** 29 %	**-** 13 s	**-**
arp3-H161A	**+** *wt*	**++** 8.3 nM	**++** 8.1 nM	**+** 12.8 s	**+/-** 134 min -0.33	**+/-** 69 %	**+/-** 89 %	**+/-** 6 s	**+**

Growth: Growth defects on different media. ss, salt sensitive; fs, formamide sensitive. Arp2 ATP hydrolysis: The concentration of Arp2 that hydrolyzed ATP in a nucleation reaction containing 10 nM Arp2/3 complex (Fig. 1c and e). Nucleation activity: The concentration of barbed ends nucleated by Arp2/3 complex in a reaction equivalent to that used to measure Arp2 ATP hydrolysis (Fig. 1e). NPF release: half-life of NPF release. Debranching: half-life (top) and plateau (bottom) of the fitted debranching curve. Note that *arp3-H161A* has a longer half-life because it has a lower plateau than either wild-type or *arp2-H161A*. Lucifer yellow internalization: Percentage of cells exhibiting Lucifer yellow staining (Fig. 2b). Sla1p internalization: The percentage of Sla1-GFP patches that exhibited inward movement (Fig. 2e). Actin disassembly: the average length of Sac6-GFP persistence after internalization. Note that *arp3-H161A* is also synthetic lethal with *cof1-22* and has slower rates of Latrunculin A-induced actin patch disassembly, leading to the +/- designation. *sla2*Δ tail formation: scored for the presence or absence of stable elongated actin tails.

Table S3. Yeast strains used in this study.

Name	Genotype	Source
DDY1810	*MATa, leu2, ura3-52, trp1, prb1-1122, pep4-3, pre1-451*	1
DDY1266	*MATα, cof1-22::URA3, leu2-3,112, ura3-52, his3Δ200, lys2-801*	2
DDY2266	*MATa, las17-16::LEU2, leu2-3,112, ura3-52, his3Δ200, lys2-801*	3
DDY2445	*MATα, arp3-G302Y::LEU2, leu2-3,112, ura3-52, his3Δ200, lys2-801*	4
DDY2447	*MATα, arp2-Y306A::URA3, leu2-3,112, ura3-52, his3Δ200, lys2-801*	4
DDY2450	*MATα, arp3-F306A::LEU2, leu2-3,112, ura3-52, his3Δ200, lys2-801*	4
DDY2457	*MATα, arp2-H161A::URA3, leu2-3,112, ura3-52, his3Δ200, lys2-801*	4
DDY2465	*MATα, arp3-H161A::LEU2, leu2-3,112, ura3-52, his3Δ200, lys2-801*	4
DDY2863	*MATa, pan1-KE101::LEU2, leu2-3,112, ura3-52, his3Δ200, lys2-801*	5
DDY2926	*MATα, ARP3::LEU2, ARC18-HA::HIS3, leu2-3,112, ura3-52, his3Δ200, lys2-801*	4
DDY2939	*MATa, SLA1-GFP::HIS3, leu2-3,112, ura3-52, his3Δ200, lys2-801*	4
DDY2954	*MATa, arp2-H161A::URA3, Arc18-HA::HIS3, leu2-3,112, ura3-52, his3Δ200, lys2-801*	6
DDY2955	*MATα, arp3-H161A::LEU2, Arc18-HA::HIS3, leu2-3,112, ura3-52, his3Δ200, lys2-801*	6
DDY2956	*MATα, arp2-H161A::URA3, Sla1-GFP::HIS3, leu2-3,112, ura3-52, his3Δ200, lys2-801*	6
DDY2957	*MATα, arp3-H161A::LEU2, Sla1-GFP::HIS3, leu2-3,112, ura3-52, his3Δ200, lys2-801*	6
DDY2958	*MATa, bbc1Δ::LEU2, Sla1-GFP::KanMX, leu2-3,112, ura3-52, his3Δ200*	6
DDY2959	*MATa, bbc1Δ::LEU2, arp2-H161A::URA3, Sla1-GFP::KanMX, leu2-3,112, ura3-52, his3Δ200*	6
DDY2960	*MATα, Sac6-GFP::HIS3, leu2-3,112, ura3-52, his3Δ200, lys2-801*	6
DDY2961	*MATα, arp2-H161A::URA3, Sac6-GFP::HIS3, leu2-3,112, ura3-52, his3Δ200*	6
DDY2962	*MATα, arp3-H161A::LEU2, Sac6-GFP::HIS3, leu2-3,112, ura3-52, his3Δ200, lys2-801*	6
DDY2963	*MATa, Sac6-RFP::HIS3, Sla1-GFP::HIS3, leu2-3,112, ura3-52, his3Δ200, lys2-801*	6
DDY2964	*MATα, arp2-H161A::URA3, Sac6-RFP::HIS3, Sla1-GFP::HIS3, leu2-3,112, ura3-52, his3Δ200, lys2-801*	6
DDY2965	*MATα, arp3-H161A::LEU2, Sac6-RFP::HIS3, Sla1-GFP::HIS3, leu2-3,112, ura3-52, his3Δ200, lys2-801*	6
DDY2966	*MATα, arp2-H161A::URA3, las17-16::LEU2, leu2-3,112, ura3-52, his3Δ200, lys2-801*	6
DDY2967	*MATα, arp2-H161A::URA3, pan1-KE101::LEU2, leu2-3,112, ura3-52, his3Δ200, lys2-801*	6
DDY2969	*MATα, sla2Δ::LEU2, Sac6-GFP::HIS3, leu2-3,112, ura3-52, his3Δ200, lys2-801*	6
DDY2970	*MATα, arp2-H161A::URA3, sla2Δ::LEU2, Sac6-GFP::HIS3, leu2-3,112, ura3-52, his3Δ200, lys2-801*	6

DDY2971	*MAT, arp3-H161A::LEU2, sla2Δ::LEU2, Sac6-GFP::HIS3, leu2-3,112, ura3-52, his3200, lys2-801*	6

1, Rodal et al, 2003. 2, Lappalainen et al, 1997. 3, Duncan et al, 2001. 4, Martin et al, 2005. 5, Toshima et al, 2005. 6, This study.